

Cross-Correlation of the 2 – 10 keV XRB with Radio Sources: Constraining the Large-Scale Structure of the X-ray Background

Stephen P. Boughn^{1,2}

¹Institute for Advanced Study, Olden Lane, Princeton, NJ 08540

²Department of Astronomy, Haverford College, Haverford, PA 19041 sboughn@haverford.edu

ABSTRACT

We present cross-correlation analyses of the HEAO 2 – 10 keV diffuse X-ray map with both the combined GB6/Parkes-MIT-NRAO (GB6-PMN) 5GHz and the FIRST 1.4GHz radio surveys. The cross-correlation functions (CCFs) of both radio surveys with the unresolved X-ray background were detected at the 5σ level. While the large angular resolution (3°) of the X-ray map makes it difficult to separate the contributions of clustering from those of Poisson fluctuations, the amplitude of the CCF provides important constraints on the X-ray emissivity of the radio sources as well as on the clustering properties of radio and X-ray sources. These constraints are subject to a number of modeling parameters, e.g. X-ray luminosity evolution, clustering evolution, the radio luminosity function, cosmological model, etc. For reasonable choices of parameters the X-ray/FIRST CCF is consistent with a correlation scale length of $6h^{-1}Mpc$. This is somewhat smaller than the scale length inferred from the autocorrelation function of the FIRST survey and implies that X-ray sources are less strongly clustered than strong radio sources, a result which is consistent with previous constraints on X-ray clustering. The X-ray/GB6-PMN CCF is several times larger and is likely to be dominated by Poisson fluctuations. This implies that $\sim 2\%$ of the diffuse X-ray background arises from the GB6-PMN sources.

Subject headings: diffuse radiation – galaxies:statistics – large-scale structure of the universe – X-rays: galaxies – X-rays: general

1. Introduction

Thirty-five years after the discovery of the cosmic X-ray background (XRB), it is still the subject of a great deal of study. On the one hand it offers the possibility of providing an extremely useful tool for the study of large scale structure in the universe (Barcons, Fabian, & Carrera 1997; Boughn, Crittenden, & Turok 1997) and yet on the other the nature and origin of the XRB is still not well understood. The deep images made by the ROSAT satellite have resolved 60% of the 0.5 – 2 keV background into discrete sources (Hasinger et al. 1993) and similar observations by the ASCA satellite have resolved 30% of the 2 – 10 keV background (Georgantopoulos et al.

1997). While it is clear that classical active galactic nuclei (AGN), i.e. QSO's, make a significant contribution to the XRB (Georgantopoulos et al. 1997; Boyle et al. 1994), it is also clear for a variety of reasons that a substantial contribution must come from some other population. $2 - 10$ keV number counts are a factor of 2 to 3 larger than inferred from $0.5 - 2.0$ keV counts if one assumes a typical AGN X-ray spectrum (Georgantopoulos et al. 1997). Indeed, the spectrum of the XRB is significantly harder than that of AGN (Gendreau et al. 1995). Finally, the strong clustering of QSO's is inconsistent with the relatively smooth XRB (Georgantopoulos et al. 1997 and references cited therein). These observations point to a large population of relatively faint (or highly absorbed) sources with hard X-ray spectra. Such sources have already begun to be identified with faint galaxies and X-ray bright, narrow emission line galaxies (Almaini et al. 1997; Almaini & Fabian 1997; Georgantopoulos et al. 1997; Refregier, Helfand, & McMahan 1997; Treyer & Lahav 1996; Roche et al. 1995). On the other hand, Comastri et al. (1995) have successfully reproduced the flux and spectrum of the XRB with a model AGN luminosity function that includes a large number of highly absorbed Seyfert 2s. In either case, if such sources make a substantial contribution then one might expect the X-ray background to be clustered more like galaxies than QSOs. This is consistent with the results of the cross-correlation analysis presented below.

In this paper we undertake cross-correlation analyses of the 'hard' ($2 - 10$ keV) X-ray background with two flux limited radio source surveys, the FIRST survey at 1.4 GHz and the combined GB6/Parkes-MIT-NRAO (GB6-PMN) surveys at 4.85 GHz. While the flux limits of these surveys differ by a factor of ~ 40 , their expected redshift distributions are similar and, therefore, the cross-correlation functions of the two surveys can be directly compared. The description of the data sets (X-ray and radio) and the editing of these sets is described in §2. The cross-correlation analysis and significance tests are described in §3. The formalism to interpret the CCF in terms of a model follows closely the analysis of Treyer and Lahav (1996) and is presented in §4. The constraints on parameters resulting from the observed CCF's are discussed in §5.

2. Data Sets

2.1. HEAO1 A2 $2 - 10$ keV X-ray Map

The HEAO1 A2 experiment measured the surface brightness of the X-ray background in the $0.1 - 60$ keV band (Boldt 1987). The present data set was constructed from the output of two medium energy detectors (MED) with different fields of view ($3^\circ \times 3^\circ$ and $3^\circ \times 1.5^\circ$) and two high energy detectors (HED3) with the same fields of view. These data were collected during the six month period beginning on day 322 of 1978. Counts from the four detectors were combined and binned in 24,576 $1.3^\circ \times 1.3^\circ$ pixels in an equatorial quadrilateralized spherical cube projection on the sky (White & Stemwedel 1992). The combined map has a spectral resolution of approximately $2 - 10$ keV (Jahoda & Mushotzky 1989). The effective point spread function (PSF) of the map

was determined by averaging the PSF’s of 75 HEAO1 point sources (Piccinotti et al. 1982). The composite PSF is well fitted by a gaussian with a full width, half maximum of 2.96° . Because of the pixelization, the PSF varies somewhat with location on the sky; however, this has little effect on the correlation analysis and so a constant PSF is used in the analysis of §4 below.

The dominant feature in the HEAO map is the Galaxy, so all data within 20° of the Galactic plane and within 30° of the Galactic center were cut from the map. In addition, 10° diameter regions around 90 discrete X-ray sources with $2 - 10 \text{ keV}$ fluxes larger than $3 \times 10^{-11} \text{ ergs}^{-1} \text{ cm}^{-2}$ (Piccinotti et al. 1982) were removed. Without this cut the CCF’s were somewhat larger and considerably more noisy due to bright, nearby Galactic and extragalactic sources. The resulting “cleaned” map covered about 50% the sky. In order to identify additional point sources, the map itself was searched for “sources” that exceeded the nearby background by a specified amount and 7° diameter regions around these were removed. Cuts were made at several levels from 4 to 10 times the photon noise. For the most extreme cuts which corresponded to a point source flux of $3 \times 10^{-11} \text{ ergs}^{-1} \text{ cm}^{-2}$ the sky coverage was reduced to about 25% of full sky. The results of these additional cuts did not significantly affect the correlation analyses and we conclude that the X-ray map contains no point sources with fluxes greater than $3 \times 10^{-11} \text{ ergs}^{-1} \text{ cm}^{-2}$. This flux cut is accounted for in the analysis of §4.

Even after cleaning, the X-ray map has several components of large-scale systemic structure which can be corrected for. If the dipole moment of the cosmic microwave background is a kinematic effect, as it has been widely interpreted (Bennett et al. 1996), then the X-ray background should possess a similar dipole structure (Compton-Getting effect) with an amplitude of 4.3×10^{-3} . Evidence for this structure is, indeed, found in the HEAO map (Shafer 1983; Lahav, Piran & Treyer 1997). The cleaned map was corrected for this effect. In addition, a linear time drift in detector sensitivity (Jahoda 1993) results in a large scale structure of known form. Finally, the $2 - 10 \text{ keV}$ background shows evidence of high latitude Galactic emission as well as emission associated with the Supergalactic plane (Jahoda 1993). Models for these contributions along with the time drift were fit to the X-ray data and subsequently subtracted from the map (Boughn, Crittenden, & Turok 1997). These contributions to the X-ray background are on large scales and have little effect on the small angular scale correlation analysis discussed below.

Because of the ecliptic longitude scan pattern of the HEAO satellite, sky coverage and, therefore, photon shot noise are not uniform. However, the mean variance of the cleaned, corrected map, $2.0 \times 10^{-2} (\text{cts/sec})^2$, is considerably larger than the mean variance of photon shot noise, $0.67 \times 10^{-2} (\text{cts/sec})^2$, where $1 \text{ cts/sec} = 2.1 \times 10^{-11} \text{ ergs}^{-1} \text{ cm}^{-2}$ (Allen, Jahoda & Whitlock 1994). This implies that the X-ray map is dominated by “real” structure (not photon shot noise). For this reason, in the correlation analyses that follow, we chose to weight each pixel equally.

2.2. FIRST 1.4 GHz Survey

The FIRST 1.4GHz survey is a continuing project to survey 10,000 square degrees of the north Galactic cap (White et al. 1997). The data used in the analysis below was obtained from the publically available catalog containing 236,177 sources from observations of 1993 through 1996. The catalog covers about 2575 square degrees and includes only sources whose peak flux exceeds 5 times the rms noise plus 0.25 mJy . Following Cress et al. (1996), all pairs of sources within 0.02 degrees of each other are considered to be part of a single doubled lobed source. For groups of three or more such sources, all sources within 0.02 degrees of the mean position of the group are considered to be part of a multi-component system and are counted as a single source. This reduces the total number of sources to 186,214. Since noise is not uniform across the coverage region, especially in those areas near very bright sources, the flux limit is not uniform. To correct for this we have flagged all map areas in which the rms noise is greater than 0.17 mJy and have removed all sources with peak fluxes less than 1.1 mJy which corresponds to a 5σ detection if $\sigma = 0.17 mJy$. This further reduces the number of sources to 163,157. It should be noted that even without the latter correction, the CCF of FIRST sources with the X-ray background is not changed significantly. This is understandable since non-uniform coverage in the FIRST catalog is not expected to be correlated with systematic structure in the X-ray map.

The remaining FIRST sources are grouped in the same $1.3^\circ \times 1.3^\circ$ pixels of the quadrilateralized cube projection used for the X-ray map. Because of flagged regions as well as the projection itself, not all pixels represent the same solid angle coverage of radio sources. Therefore, the radio coverage of each pixel is used to weight its contribution to the cross-correlation in a way so as not to bias the result. See §3 below. The number of pixels that contain FIRST data is 1696; although, somewhat less, 1100, are common to both the FIRST and X-ray maps.

2.3. Parkes-MIT-NRAO and GB6 4.85 GHz Surveys

The publically available Parkes-MIT-NRAO (PMN) southern sky survey was made with the 64-m radio telescope at Parkes, NSW, Australia, and contains about 50,000 sources (Wright et al. 1994; Griffith et al. 1994; Griffith et al. 1995; Wright et al. 1996). The flux limit in this combined survey is not uniform but varies from 20 mJy to 72 mJy . As a compromise between uniform coverage and total number of sources we chose to use a 50 mJy flux limited sample and flagged all portions of the sky not covered to that level. This required excluding the Zenith zone of the survey. In addition, only those sources with $Dec < 0^\circ$ were included since the northern sources overlapped with the GB6 survey. Following Loan, Wall, & Lahav (1997) we excluded several small regions with extended sources. Finally all regions of the sky within 20° of the Galactic plane and within 30° of the Galactic center were removed from consideration. After these cuts 15,233 sources remain in the catalog.

The Green Bank 6cm (GB6) survey of the northern sky ($0^\circ < Dec < 75^\circ$) was made with

the NRAO 91m telescope during 1986-7 and contains 75,162 sources brighter than $\sim 18mJy$ (Gregory et al. 1996). Rather than worry about comparing the flux calibrations of the GB6 and PMN surveys we chose a somewhat smaller flux limit for the GB6 survey, $45mJy$, which resulted in the equality of the surface density of sources ($1.50deg^{-2}$) in the two maps. In any case, the correlation analysis below was performed on the two surveys separately as well as on the combined GB6-PMN survey.

The combined GB6-PMN flux limited sources were also grouped in the same $1.3^\circ \times 1.3^\circ$ pixels as the X-ray map. There are $\sim 34,000$ sources and 13,520 pixels in the combined map which corresponds to 55% sky coverage; although, only 10,115 pixels are common to both the GB6-PMN and cleaned X-ray maps.

3. Cross-Correlation Functions

We define the dimensionless cross-correlation function of the X-ray intensity, I , with the radio source number, N , as

$$W(\theta)_{I,N} = \frac{\sum_{i,j} (I_i - \bar{I})(N_j - \bar{N}_j)}{\sum_{i,j} \bar{I}\bar{N}_j} \quad (3-1)$$

where the sum is over all pairs of pixels, i, j , separated by an angle θ , \bar{I} is the mean X-ray intensity, and \bar{N}_j is the mean number of radio sources in the j^{th} pixel. As discussed in §2.2, the FIRST radio coverage of each $1.3^\circ \times 1.3^\circ$ pixel is not the same. Therefore, we take $\bar{N}_j = \bar{n}\Omega_j$ where \bar{n} is the mean surface density of radio sources and Ω_j is the solid angle of radio coverage of the j^{th} pixel.

Figures 1 and 2 are the CCFs of the 2 – 10 keV HEAO map with the combined GB6 and PMN surveys and with the FIRST survey. Although, the CCFs are shown out to separation angles of 15° , a significant signal is only detected in the first few bins. The errors were computed using a “bootstrap” analysis (Cress et al. 1996; Fisher et al 1994; Ling, Frenk & Barrow 1986). 100 random radio source catalogs, each of the same size as the original catalog were generated by choosing sources at random from the original catalog. Note that this requires some sources will be chosen more than once. These random catalogs are then cross-correlated with the real X-ray map according to equation (3-1). The mean CCF of the random trials was consistent with that of the real data and the rms fluctuation about the mean CCF provides an estimate of the uncertainty due to the additional Poisson noise in the distribution of radio sources.

For the FIRST/X-ray CCF, the error estimates were checked in two ways. A series of 59 radio source maps were generated by a reflection through the celestial equator followed by a rotation about the celestial pole in 6° increments. These radio maps were then cross-correlated with the X-ray map which was first transformed into Galactic coordinates. This latter transformation resulted in a pixel coverage nearly the same as that of the original data for small separation angles. The resulting transformed X-ray and radio maps possessed little small-scale correlation. The rms scatter of the CCF’s of this set of maps agreed with the bootstrap error estimates for

$\theta < 3^\circ$ and was about 50% larger than the bootstrap estimates for $\theta > 3^\circ$. An additional rough error estimate was obtained by dividing the two data sets in half and comparing the CCFs of both halves. For two different partitions, north-south and east-west, the differences in the two CCFs were consistent with the quoted errors. Both these estimates imply that the bootstrap error estimates are reasonable. We consider the bootstrap error estimates preferable in that they reflect the actual distribution of data on the sky. To compare the consistency of the GB6 and PMN portions of the $5GH_z$ map, the CCF was computed separately for each and the results are plotted in Figure 3. It is clear that they are consistent with each other (and with Figure 1) to within the estimated errors.

Figures 1 and 2 demonstrate that there is a statistically significant cross-correlation of radio source counts and the $2 - 10 keV$ background at the 5σ level. It may appear from the figures that the significance is higher than this; however, because of the X-ray PSF, the error bars are highly correlated. The correlation coefficients of adjacent errors are typically between 0.4 and 0.7.

Also evident in Figures 1 and 2 is that for $\theta \leq 2^\circ$ the GB6-PMN/X-ray CCF exceeds the FIRST/X-ray CCF by a factor of ~ 3 . In addition, it appears that the latter CCF is more extended than the former. It is possible that these two properties are related. It will be shown in §4 that the finite PSF of the X-ray map results in a $W(\theta)$ profile similar to that of the GB6-PMN/X-ray CCF even if the only cross-correlation arises from the Poisson noise in individual sources. To the extent that the GB6-PMN/X-ray CCF is dominated by Poisson noise it will be both larger in amplitude and more narrow in angular scale than a CCF for which Poisson noise is negligible. We suggest in §4 that this is the case here.

4. Interpretation of the Cross-Correlation Function

The observed $W(\theta)$'s in §3, depend on the properties of radio sources and X-ray sources, the spatial clustering of these populations, and the large scale geometry of the universe. Among the quantities included in the following model of $W(\theta)$ are the luminosity function of the radio sources, the luminosity (and density) evolution of radio sources, the X-ray luminosity of radio sources, the spectrum and evolution of X-ray emissivity, the functional form and evolution of the spatial cross-correlation function, and the cosmological parameters, H_o and q_o . Although these parameters provide considerable freedom in fitting the observed $W(\theta)$, the constraints placed on parameter space are reasonably strong. The analysis of this section follows closely that of Treyer and Lahav (1996). The reader is referred to that paper for a detailed analysis.

Let η_o be the unnormalized, angular cross-correlation function. If the sky is divided up into cells of small solid angle ω , then

$$\eta_o = \langle \delta N \delta I \rangle = \langle (N - \langle N \rangle)(I - \langle I \rangle) \rangle = \langle NI \rangle - \langle N \rangle \langle I \rangle \quad (4-1)$$

where N and I are the number of radio sources in and average X-ray intensity of each cell, and the

average is over all cells. It is straightforward to show that (Treyer & Lahav 1996; Peebles 1980)

$$\langle NI \rangle = \int \frac{\varepsilon_r}{4\pi r_L^2} dV + \int \int n(\mathbf{r}_1) \frac{\varepsilon_b(\mathbf{r}_2)}{4\pi r_{L_2}^2} [1 + \xi(r_{12})] dV_1 dV_2 \quad (4-2)$$

and

$$\langle N \rangle \langle I \rangle = \int n(\mathbf{r}_1) dV_1 \int \frac{\varepsilon_b(\mathbf{r}_2)}{4\pi r_{L_2}^2} dV_2 \quad (4-3)$$

where ε_r and ε_b are the comoving volume X-ray emissivities of the radio source population and the total X-ray background respectively, n is the comoving number density of radio sources, r_L is the luminosity distance, and the integrals are performed over the comoving volumes subtended by the solid angle ω of the cell. $\xi(r_{12})$ is the spatial cross-correlation function of radio sources with the X-ray background in regions of space separated by a proper distance r_{12} , i.e.

$$\langle n(\mathbf{r}_1) \varepsilon_b(\mathbf{r}_2) \rangle = [1 + \xi(r_{12})] \langle n \rangle \langle \varepsilon_b \rangle \quad (4-4)$$

Thus $\eta_o = \eta_P + \eta_c$ where

$$\eta_P = \int \frac{\varepsilon_r}{4\pi r_L^2} dV \quad (4-5)$$

and

$$\eta_c = \int \int n(\mathbf{r}_1) \frac{\varepsilon_b(\mathbf{r}_2)}{4\pi r_{L_2}^2} \xi(r_{12}) dV_1 dV_2 \quad (4-6)$$

The first term, η_P , arises from Poisson fluctuations due to the X-ray emission of the individual radio sources and is equal to the X-ray flux from these sources, i.e.,

$$\eta_P = \omega \bar{I}_r \quad (4-7)$$

where \bar{I}_r is the mean X-ray intensity of the radio sources. The second term, η_c , is due to the joint clustering of radio sources with the sources of the X-ray background (including the radio sources).

The spatial auto-correlation function (ACF) of nearby galaxies is well approximated by a power law. We take this form for the spatial cross-correlation function and assume the standard power law evolution (Peebles 1980)

$$\xi(r, z) = (1 + z)^{-(3+\epsilon)} \left(\frac{r}{r_o} \right)^{-\gamma} \quad (4-8)$$

where r is the proper (non-comoving) distance between the sources, r_o is the comoving correlation length, and ϵ is a clustering evolution parameter. For ‘stable’ clustering $\epsilon = 0$ while $\epsilon = \gamma - 1$ for linearly growing perturbations in an Einstein-de Sitter universe (Treyer & Lahav 1996). Because the correlation scale length r_o is small, i.e. $\sim 10 Mpc$, sources at significantly different redshifts are uncorrelated. In this case the integrals in equation (4-6) can be simplified to a single integral over redshift (Treyer & Lahav 1996),

$$\eta_c = K_\gamma H_\gamma r_o^\gamma \int \frac{n(z) \varepsilon_b(z)}{4\pi r_L(z)^2} (1 + z)^{-(3+\epsilon)+\gamma} r_c(z)^{5-\gamma} F(z) dr_c(z) \quad (4-9)$$

where $K_\gamma = \int d\Omega_1 \int d\Omega_2 \theta_{12}^{1-\gamma}$; θ_{12} is the angle between θ_1 and θ_2 ; $H_\gamma = \Gamma(\frac{1}{2})\Gamma(\frac{\gamma-1}{2})/\Gamma(\frac{\gamma}{2})$; r_c is the comoving radial coordinate; and $F(z)r_c^2 dr_c d\Omega \equiv dV$. This expression can be further simplified by noting that $r_L(z) = (1+z)r_c(z)$ and $n(z)dV/d\Omega = n(z)F(z)r_c^2 dr_c = N(z)dz$ where $N(z)dz$ is the surface density of radio galaxies at redshift z . Following Treyer & Lahav (1996) we assume a power law evolution of the *observed* XRB volume emissivity, i.e. $\varepsilon_b(z) = \varepsilon_{b,o}(1+z)^q$. Note that q includes the “K-correction” exponent, $1 + \alpha$, where α is the energy spectral index. Then the expression for η_c becomes

$$\eta_c = \frac{K_\gamma H_\gamma r_o^\gamma \varepsilon_{b,o}}{4\pi} \int N(z)(1+z)^{\gamma+q-5-\epsilon} r_c(z)^{1-\gamma} dz \quad (4-10)$$

Equations (4-7) and (4-10) give the value of the cross-correlation at zero separation for an X-ray map with a delta function PSF. It is straightforward to show that for a finite PSF and for arbitrary separation angle, θ , η_P becomes

$$\eta_P(\theta) = B(\theta)\bar{I}_r \quad (4-11)$$

where

$$B(\theta) = \int_{radio} P(\theta - \theta') d\Omega', \quad (4-12)$$

$P(\theta')$ is the normalized PSF, i.e., $\int P(\theta') d\Omega' = 1$, the integration is over the radio cell, and θ is the location of the X-ray cell relative to the radio cell. The expression for $\eta_c(\theta)$ is again equation (4-10) if K_γ is substituted with

$$K_\gamma(\theta) = \int_S d\Omega_1 P(\theta_1) \int_{radio} d\Omega_2 \theta_{12}^{1-\gamma} \quad (4-13)$$

where \int_S indicates an integral over all space. These two expressions are equivalent to those derived by Refregier, Helfand, and McMahon (1997) recalling that the effective PSF used here is the actual PSF averaged over an X-ray cell. It should be noted that, due to the finite PSF, the Poisson term contributes to the CCF for $\theta > 0$. Of course, this is why it is problematic to distinguish real clustering from Poisson fluctuations.

As an illustration, Figures 1 and 2 show a fit of $B(\theta)$ to the GB6-PMN/X-ray CCF and a fit of $K_\gamma(\theta)$ to the FIRST/X-ray CCF. We have chosen $\gamma = 2.0$ to evaluate K_γ which is consistent with the auto-correlation function of FIRST sources found by Cress et al. (1996) and similar to the value ($\gamma = 1.8$) for local bright galaxies (Peebles 1980). Weighted least squares fits to the first 4 data points were performed following a similarity transformation to diagonalize the noise matrix. As long as the first three points are included, the results are rather insensitive to the number of points included. Because of the pixelization of the data, theoretical functions $K_\gamma(\theta)$ and $B(\theta)$ are evaluated at only those angles appropriate for the data. For aesthetic reasons, these points are connected by straight lines in the Figures. Both of the curves look reasonable for $\theta < 5^\circ$. For $\theta > 5^\circ$, the data of Figure 2 fall consistently below the theoretical curve. This is not unexpected since 5° corresponds to rather large distances at even modest redshifts, e.g. at $z = 0.2$ an angle of 5° corresponds to $44h^{-1} Mpc$ for an Einstein-de Sitter universe. On the other hand the observed galaxy ACF displays a break below the power law at lengths $\gtrsim 30h^{-1} Mpc$ (Peebles

1993). This behavior is consistent with the evolution of very large scale structure in a standard CDM universe (see e.g. Padmanabhan 1993). As an indication of the magnitude of this effect we have constructed a theoretical CCF from equation (4.6) with the power-law $\xi(r_{12})$ cutoff above $r_{12} = 30h^{-1}Mpc$. Figure 4 is a fit of this profile to the FIRST/X-ray CCF. The discrepancy at large angles is no longer egregious while the amplitude of the fit is nearly the same as in Figure 2. We make no claim that this model has any particular significance but offer it as an indication of the magnitude of the effect.

The formal χ_ν^2 for the two fits in Figures 1 & 2 are 0.2 and 1.7 respectively for three degrees of freedom. On the other hand, fits of $K_\gamma(\theta)$ to the GB6-PMN/X-ray CCF and of $B(\theta)$ to the FIRST/X-ray CCF give $\chi_\nu^2 = 6.2$ and 7.3. Fitting the $B(\theta)$ and $K_\gamma(\theta)$ profiles simultaneously to the two CCFs doesn't improve χ_ν^2 and, in fact, is consistent with no $B(\theta)$ contribution to the FIRST data and no $K_\gamma(\theta)$ contribution to the GB6-PMN data. These results are suggestive that the GB6-PMN CCF is Poisson dominated while the FIRST CCF is clustering dominated. The conclusions are not overly sensitive to γ . If γ is chosen to be that found for the ACF of nearby galaxies (Peebles 1980), i.e., $\gamma = 1.8$, the fit of K_γ to the FIRST CCF is somewhat worse ($\chi_\nu^2 = 2.3$) while the K_γ profile is even more inconsistent ($\chi_\nu^2 = 9.4$) with the the GB6-PMN CCF. These matters will be discussed further in §5.

In order to compare the amplitudes of the predicted $\eta_o(\theta)$ with the observed $W(\theta)$ s, a number of parameters must be specified: γ , q , $\varepsilon_{b,o}$, ϵ , r_o , and z_{cutoff} , the redshift at which X-ray sources “turn on” and thus the upper limit to the integral in equation (4-10). The functions $r_c(z)$ and $F(z)$ require an assumption about the large-scale geometry of the universe, and the distribution of radio sources $N(z)$ depends on the evolving luminosity function of radio sources as well as on the geometry of the universe.

In the analysis that follows $N(z)$ is computed from the fundamental “free-form model” of the radio luminosity function of Dunlop & Peacock (1990) with low flux cutoffs appropriate to the two surveys. Figures 5 and 6 are the $N(z)$ s computed from this model for the GB6-PMN and FIRST surveys. For the $1.1mJy$ peak flux cut in the FIRST survey, the effective completeness flux is about $1.5mJy$ (Becker, White & Helfand 1995; White et al. 1997). We have repeated the analyses using the evolving luminosity and number density model of Dunlop & Peacock and, although the $N(z)$ s are somewhat different, the differences in the correlation analyses are small. Because $N(z)$ falls off at large redshift, the computed values of η_c are rather insensitive to z_{cutoff} ; however, this parameter is important in constraining X-ray emissivity.

The emissivity $\varepsilon_{b,o}$ of the X-ray background must satisfy the constraint that the integrated intensity equal that observed for the $2 - 10 keV$ background, i.e. $5.1 \times 10^{-8} ergs^{-1} cm^{-2} sr^{-1}$ (Marshall et al. 1980). For a given evolution parameter q and cosmological model, $\varepsilon_{b,o}$ is uniquely determined. In principle, q could be determined uniquely from the observed local X-ray emissivity; however, uncertainty in this value as well as uncertainty in z_{cutoff} result in considerable uncertainty in q . In addition, it is quite likely that a simple power law evolution is not the

best description of X-ray emissivity. If one arbitrarily sets $z_{cutoff} = 4$, then, for an Einstein-de Sitter universe, the local X-ray emissivities implied for $q = 2, 3, 4$ are 18.7, 8.3, and $3.0 \times 10^{38} h \text{ ergs}^{-1} \text{ Mpc}^{-3}$ where $h = H_o/100 \text{ kms}^{-1} \text{ Mpc}^{-1}$. The locally measured value is $8.6 \pm 2.4 \times 10^{38} h \text{ ergs}^{-1} \text{ Mpc}^{-3}$ for AGN alone with an upper limit of $4 \times 10^{38} h \text{ ergs}^{-1} \text{ Mpc}^{-3}$ for the contribution of weaker sources (e.g. star-forming galaxies, LINERS) (Miyaji et al. 1994). It appears that for power law evolution models, q is constrained to fall between 2 and 4. As a somewhat more sophisticated model of evolution we consider the unified AGN model of Comastri et al. (1995) which reproduces both the amplitude and spectrum of the XRB. Figure 7 is a plot of the redshift distribution of the X-ray intensity, $\mathcal{F}(z) \equiv dI/dz$, from the Comastri et al. model with the flux cut $3 \times 10^{-11} \text{ erg s}^{-1} \text{ cm}^{-2}$ appropriate for the present X-ray map (Boughn, Crittenden, & Turok 1997). Expressed in terms of \mathcal{F} , equation (4-10) must be modified slightly,

$$\eta_c = K_\gamma H_\gamma r_o^\gamma \int \frac{\mathcal{F}(z)N(z)}{F(z)dr_c/dz} (1+z)^{\gamma-3-\epsilon} r_c(z)^{1-\gamma} dz. \quad (4-14)$$

For the special case of an Einstein-de Sitter universe ($\Omega_o = 1$) this equation becomes

$$\eta_c = \frac{K_\gamma(\theta)H_\gamma r_o^\gamma}{2^{\gamma-1}(c/H_o)^\gamma} \int \mathcal{F}(z)N(z)(1+z)^{\gamma-\frac{3}{2}-\epsilon} r_c(z)[1+(1+z)^{-\frac{1}{2}}]^{1-\gamma} dz \quad (4-15)$$

where H_o is Hubble's constant and c is the speed of light.

The η_c computed using this model is intermediate between those of the $q = 3$ and $q = 4$ power law models. We note that the redshift distribution of the X-ray 2 – 10 keV intensity for the Comastri et al. model is relatively flat and that a $q = 3.5$ power law evolution gives a flat redshift distribution. In the analysis that follows, we will use the Comastri et al. model for the evolving X-ray emissivity as our “best guess” but will compare the results of this model with those of $q = 2, 3, 4$ power law models.

Because of the large angular resolution (3°) of the HEAO map, most of the contribution to the CCF arises from nearly linearly evolving structures. At $z = 0.2$, 1° corresponds to $9h^{-1} \text{ Mpc}$ which is comparable to the transition from the linear to non-linear regime in the local universe. In the “best guess” model below, roughly 50% of the contribution to the CCF comes from redshifts below $z = 0.2$ where evolution is modest and 50% comes from redshifts $z > 0.2$ where 1° is in the linear regime. For this reason we assume for our “best guess” model that structure is growing linearly in an Einstein-de Sitter universe, i.e., $\epsilon = \gamma - 1$. However, the change in the results if the clustering is stable, i.e., $\epsilon = 0$ and for open and “ Λ ” universes will be discussed.

Finally one must take into account the flux limit ($3 \times 10^{-11} \text{ ergs}^{-1} \text{ cm}^{-2}$) on X-ray sources. There is no well-defined procedure to do this for the power law models of emissivity evolution since individual source luminosities are not specified. However, the flux cut can be directly applied to the Comastri et al. model and we have done so. The net result is to roll off the X-ray flux at $z < 0.05$. To the extent that faint (non-AGN) X-ray sources contribute significantly to the X-ray background this results in an underestimate of η_c . We take the lower limit of the η_c integral to be

$z = 0.01$ ($30h^{-1}Mpc$). This has the effect of a flux cut for the power law models but in any case it has little effect on the integral.

Figure 8 is a plot of the computed $\eta_c(0)$ as a function of the correlation scale length r_o for parameters of both the GB6-PMN and FIRST data sets. Although the predicted number densities, $N(z)$, of the Dunlop & Peacock model are within 15% of the observed values ($1.50/deg^2$ for GB6-PMN and $57.3/deg^2$ for FIRST), the models were renormalized to agree with the observed values. All other parameters were taken from the “best guess” model, i.e. $\gamma = 2.0$, $\epsilon = 1$, Einstein-de Sitter universe, Comastri et al. X-ray emissivity model (roughly equivalent to $q = 3.5$). The horizontal lines in Figure 8 are the amplitudes of the observed CCFs got from fitting the $W(\theta)$ s of §3 to the functional form of $K_\gamma(\theta)$. The formal errors in these fits are on the order of 20%; however, recall that in the case of GB6-PMN the χ^2 of the fit was not good. The implications are discussed in §5.

The uncertainties in the model curves were not indicated in Figure 8 because they are not well known. However we now discuss how varying parameters quantitatively changes the curves. In all cases, except for varying γ , the curves are simply displaced vertically. If one substitutes the power law evolution model for the Comastri et al. model for the XRB the values for η_c are changed by factors of 2.5, 1.4, and 0.7 for $q = 2, 3, \text{ and } 4$ respectively. Although we have argued that linear clustering growth is appropriate for the current analysis, for stable clustering evolution, i.e. $\epsilon = 0$, η_c is larger by a factor of ~ 1.5 . In the extreme case, non-evolving clustering in the comoving frame, i.e., $\epsilon = -1$, η_c is increased by a factor of ~ 2.6 .

A change in the value of γ in our “best guess” model changes the slope as well as the amplitude of the model curves in Figure 8. If $\gamma = 1.8$, the value observed for nearby galaxies (Peebles 1980), the value of $\eta_c(0)$ for $r_o = 5h^{-1}Mpc$ is a factor of ~ 1.3 larger than in Figure 8. Because of the different scale length dependence, there is an r_o above which the modified $\eta_c(0)$ will be less than the “best guess” value. This value is $16h^{-1}Mpc$. If in addition one includes stable clustering the multiplicative factor is ~ 1.8 and the corresponding crossover r_o is $100h^{-1}Mpc$.

To access the dependence of η_c on the radio luminosity function we have recomputed η_c for the density/luminosity evolution model of Dunlop & Peacock (1990). This and the previous free-form model represent the spread in the models considered by Dunlop & Peacock. The dependence is not large. For the GB6-PMN parameters η_c decreases by a factor 0.92 while for the FIRST parameters η_c increases by a factor of 1.1. Both of these radio luminosity functions predict a large number of low luminosity ($\leq 10^{30}ergs^{-1}Hz^{-1}$) radio sources and the value of η_c contains a non-negligible contribution from these sources. The contribution to η_c from radio sources with luminosities $\nu L_\nu \leq 3 \times 10^{39}ergs^{-1}$ is 6% for the GB6-PMN data and 30% for the FIRST data. The possible significance of this rather large contribution will be discussed in §5.

Finally, we investigated the dependence of the analyses on the large-scale geometry of the universe. For open ($\Lambda = 0$) universes, the value of η_c increases somewhat, a factor of ~ 1.3 for an $\Omega_o = 0.1$ universe and a factor of ~ 1.1 for an $\Omega_o = 0.3$ universe. For flat, lambda universes, the

factors are ~ 0.83 for the $\Omega_o = 0.1$ universe and ~ 0.85 for the $\Omega_o = 0.3$ universe.

5. Discussion

We begin by considering the fits of our “best guess” model to the two data sets as indicated in Figures 1 and 2. For the FIRST data this implies that $W(0) = \eta_c(0)/\langle N \rangle \langle I \rangle = 4.9 \pm 0.9 \times 10^{-4}$ or $\eta_c(0) = 2.4 \pm 0.4 \times 10^{-9} \text{ ergs}^{-1} \text{ cm}^{-2} \text{ sr}^{-1}$ where $W(0)$ is the fitted amplitude of the angular CCF. This value is indicated by a horizontal line in Figure 8 and implies a cross-correlation scale length r_o of $5.7 \pm 0.5 h^{-1} \text{ Mpc}$ where the error is the statistical error of the fit. It was found in §4 that varying the model parameters from the “best guess” values most often results in an increase in the predicted value of $\eta_c(0)$ and, therefore, a decrease in the value of r_o inferred from the observed CCF. For power law models of the evolution of the X-ray emissivity, only for $q \geq 3.5$ does the predicted value of r_o exceed the value implied by the “best guess” model and such models imply a local X-ray emissivity below that observed. Therefore, we consider that, with two caveats, $5.7 \pm 0.5 h^{-1} \text{ Mpc}$ is an upper limit to the cross-correlation scale length. The first caveat is that the Dunlop-Peacock radio luminosity function does not seriously overestimate the number of low luminosity sources. If it does then the predicted η_c will decrease and the implied scale length increase accordingly. The other caveat is that the universe has a vanishing cosmological constant. In a flat, low Ω_o universe the implied r_o is increased by about 10%.

If the Poisson term, η_P , makes a significant contribution to the FIRST/X-ray CCF then the implied value of η_c is smaller which in turn lowers the estimate of r_o . Suppose that half the amplitude of the observed $W(0)$ is due to Poisson fluctuations. Correcting for these fluctuations and fitting the clustering term to the residuals implies a clustering amplitude of $\eta_c(0) = 1.9 \pm 0.4 \times 10^{-9} \text{ ergs}^{-1} \text{ cm}^{-2} \text{ sr}^{-1}$ and a correlation scale length of $5.0 \pm 0.5 h^{-1} \text{ Mpc}$. It seems unlikely that the Poisson contribution could be more than this and still be consistent with the observed $W(\theta)$.

The fitted amplitude of $\eta_c(\theta)$ to the GB6-PMN data implies $r_o = 10 \pm 2 h^{-1} \text{ Mpc}$; however, as pointed out in §4 the $W(\theta)$ profile of this data indicates that Poisson fluctuations dominate and, therefore, this value is clearly an overestimate. Assuming that the observed CCF is entirely due to Poisson fluctuations, the fitted amplitude of the angular CCF is (see Figure 1) $W(0) = 1.7 \pm 0.3 \times 10^{-3}$. From Equation (4-11)

$$W(0) = \frac{\eta_P(0)}{\langle N \rangle \langle I \rangle} = \frac{B(0) \bar{I}_r}{\langle N \rangle \langle I \rangle} \quad (5-1)$$

where $\langle I \rangle$ is the mean intensity of the X-ray background and \bar{I}_r is the mean X-ray intensity of the radio sources in the survey. Therefore, the fraction of the XRB that is accounted for by the survey radio sources is given by

$$\frac{\bar{I}_r}{\langle I \rangle} = \frac{W(0) \langle N \rangle}{B(0)}. \quad (5-2)$$

Substituting the inferred value of $W(0)$ in this expression implies that 2.7% of the XRB is due to GB6-PMN radio sources. This is, of course, an overestimate because clustering has not been taken into account. A better estimate is got by assuming the GB6-PMN/X-ray data has the same normalized clustering as that of the FIRST/X-ray data, i.e. $W(0) = 4.9 \times 10^{-4}$. Subtracting this from the GB6-PMN/X-ray CCF and fitting the residuals to η_P gives a Poisson amplitude of $W_P(0) = 1.3 \times 10^{-3}$ which implies 2.1% of the XRB is due to GB6-PMN radio sources. It seems unlikely that the fraction of radio source contribution to the X-ray background could be much less than 2% without requiring a much larger clustering contribution than is allowed by the observed $W(\theta)$ profile. We note in passing that under the assumptions that the radio number counts have a Euclidean dependence on radio flux S , i.e., $N(> S) \propto S^{-\frac{3}{2}}$, and that the average X-ray to radio luminosity is independent of redshift, the contribution of radio sources to the X-ray background saturates at $S = 20\mu Jy$. We hasten to add, however, that neither of these assumptions is likely to be true.

The profile of the FIRST/X-ray CCF is consistent with no Poisson fluctuations. However, if we assume that half the amplitude $W(0)$ of the observed CCF is due to Poisson fluctuations then the implied contribution of the FIRST sources to the XRB is $\sim 20\%$. We consider this to be an upper limit.

Treyer and Lahav (1996) suggested that cross-correlation analyses of the type above might enable one to map the X-ray volume emissivity as a function of redshift. Unfortunately, the current result is not very useful in this regard. Although the mean redshift of the two radio surveys is quite large, $z \sim 1$, the primary contributions to the CCF comes from lower redshifts, i.e. $\sim 50\%$ from $z < 0.2$. The result is that the CCF analysis is not very sensitive to the evolution of emissivity. For example, the η_c for a model with non-evolving emissivity, $\varepsilon_b = 9.6 \times 10^{38} h \text{ erg } s^{-1} Mpc^{-3}$, is the same as the η_c for our “best guess” model. Although such a model is wildly inconsistent with the level of the XRB, it is quite consistent with both the observed CCF and local X-ray emissivity (Miyaji et al. 1994).

Thus far only upper limits on the clustering of the hard X-ray background have appeared in the literature. We are left with the question of how to interpret the cross-correlation reported in this paper. If one assumes “linear biasing” then

$$\frac{\delta\rho}{\rho} = \frac{\delta n_r}{b_r n_r} = \frac{\delta\varepsilon_x}{b_x \varepsilon_x} \quad (5-3)$$

where ρ is mass density, n_r is radio source density, ε_x is X-ray volume emissivity, δ indicates *rms* fluctuations in these quantities, and b_r and b_x are the radio and X-ray bias factors. To the extent that the bias factors are independent of scale, the spatial ACFs of the quantities are related by

$$\xi_m(r) = \xi_r(r)/b_r^2 = \xi_x(r)/b_x^2. \quad (5-4)$$

If $\xi(r) \propto (\frac{r}{r_0})^{-\gamma}$, then $r_{o,r} \propto b_r^{\frac{2}{\gamma}}$ and $r_{o,x} \propto b_x^{\frac{2}{\gamma}}$. Then the cross-correlation function satisfies

$$\xi_{rx} = \frac{\langle \delta n_r \delta \varepsilon_x \rangle}{n_r \varepsilon_x} \propto b_r b_x \propto (r_{o,r} r_{o,x})^{\frac{\gamma}{2}}. \quad (5-5)$$

Assuming that $\xi_{rx} \propto (\frac{r}{r_{o,xr}})^{-\gamma}$, the cross-correlation scale length, $r_{o,xr}$ is equal to the geometric mean of the two auto-correlation scale lengths, i.e.,

$$r_{o,xr} = (r_{o,r}r_{o,x})^{\frac{1}{2}}. \quad (5-6)$$

While it is likely that both of these assumptions are violated to some extent, it seems reasonable that equation (5-6) is a valid approximation.

The expression for the unnormalized ACFs for X-ray flux and radio source counts is equation (4-15) with $\mathcal{F}(z)N(z)$ replaced by either $\mathcal{F}(z)^2$ for the X-ray ACF or $N(z)^2$ for the radio ACF. If the PSF is a delta function and the cell size is small, the expression for $K_\gamma(\theta)$ becomes $K_\gamma(\theta) = \theta^{1-\gamma}\omega^2$ (Treyer & Lahav 1996) where ω is the solid angle of a cell. Then

$$\eta_{ACF} = H_\gamma r_o^\gamma \theta^{1-\gamma} \omega^2 \int f(z)^2 (1+z)^{\gamma-\frac{3}{2}-\epsilon} [1 - (1+z)^{-\frac{1}{2}}]^{1-\gamma} dz \quad (5-7)$$

where $f(z)$ is either $N(z)$ or $\mathcal{F}(z)$. To obtain the normalized ACFs one must divide by either $\langle N \rangle^2$ or $\langle I \rangle^2$ where $\langle N \rangle$ or $\langle I \rangle = \omega \int f(z) dz$. Thus

$$W_{ACF}(\theta) = H_\gamma r_o^\gamma \theta^{1-\gamma} \frac{\int f(z)^2 (1+z)^{\gamma-\frac{3}{2}-\epsilon} [1 - (1+z)^{-\frac{1}{2}}]^{1-\gamma} dz}{(\int f(z) dz)^2}. \quad (5-8)$$

The strongest limit on the 2–10 keV ACF is from Carrera et al. (1993) where the 2σ limit at $\theta = 2^\circ$ is $W_x(2^\circ) < 5 \times 10^{-4}$. Substituting this value into equation (5-8) and using our “best guess” model for the XRB we find that $r_{o,x} < 7h^{-1} Mpc$. Cress et al. (1996) have recently measured the radio ACF for the initial FIRST data release (about half the number of sources used in this paper). From their Figure 1 we find that $W_r(2^\circ) \sim 2 \times 10^{-3}$. Again substituting this value and the “best guess” model parameters into equation (5-8) we find that $r_{o,r} \sim 10h^{-1} Mpc$. This value agrees with their preliminary reported value (Cress et al. 1996). Substituting these values of $r_{o,x}$ and $r_{o,r}$ into equation (5-6) implies a constraint on the cross-correlation length of $r_{o,xr} \lesssim 8h^{-1} Mpc$ which is consistent with our observed value of $\lesssim 6h^{-1} Mpc$. On the other hand, substituting $r_{o,r} \approx 10h^{-1} Mpc$ and $r_{o,xr} \lesssim 6h^{-1} Mpc$ into equation (5-6) yields $r_{o,x} \lesssim 4h^{-1} Mpc$ which is smaller than the correlation length of galaxies. This is somewhat bothersome and may imply that either we have underestimated the cross-correlation length scale or that $r_{o,r} \approx 10h^{-1} Mpc$ is an overestimate. The latter will undoubtedly be clarified as more of the FIRST survey is completed.

Finally, we pointed out in §4 that the estimate of $r_{o,xr}$ would be increased if low luminosity radio sources are significantly overestimated by the Dunlop-Peacock models. However, the implied constraint on $r_{o,x}$ is relatively insensitive to the luminosity function. For example, if we artificially cut off the radio luminosity function at $\nu L_\nu = 10^{40} erg s^{-1}$ the inferred limit of $r_{o,xr}$ increases to $\lesssim 8h^{-1} Mpc$ while $r_{o,r}$ becomes $15h^{-1} Mpc$. Then equation (5-6) still implies that $r_{o,x} \lesssim 4h^{-1} Mpc$.

6. Conclusions

The $2 - 10$ keV X-ray background (at 3° angular resolution) is significantly correlated with both 1.4 GHz FIRST radio source counts and 5 GHz GB6 and Parkes-MIT-NRAO radio source counts. The amplitude of the cross-correlation functions for these two data sets is $W_{xr}(0) = 4.9 \pm 0.9 \times 10^{-4}$ for the FIRST/X-ray CCF and $W_{xr}(0) = 1.7 \pm 0.3 \times 10^{-3}$ for the GB6-PMN/X-ray CCF. Interpreted in terms of a “best guess” model ($\Omega_o = 1$, linear growth of perturbations, Dunlop-Peacock radio luminosity function, and a unified AGN model of the XRB), the FIRST/X-ray CCF implies a comoving correlation length of $r_{o,xr} = 5.7 \pm 0.5 h^{-1} Mpc$ (statistical error only). The dependence of this value on model parameters indicates that a reasonable upper limit to the correlation length is $r_{o,xr} \lesssim 6h^{-1} Mpc$. If the FIRST ACF correlation length is $r_{o,r} \approx 10h^{-1} Mpc$ as has been reported, then the implied XRB ACF correlation length is $r_{o,x} \lesssim 4h^{-1} Mpc$ which is somewhat smaller than the galaxy-galaxy correlation length, $5h^{-1} Mpc$. We note in passing that if $r_{o,r} \sim 7h^{-1} Mpc$ then the implied X-ray correlation length is $r_{o,x} \sim 5h^{-1} Mpc$ and we suggest that future radio observations may reveal the smaller ACF implied by this value. In any case, a low value of the X-ray correlation length, $\lesssim 5h^{-1} Mpc$, is consistent with the hypothesis that a significant fraction of the XRB is due to objects which are less strongly clustered than luminous AGNs, i.e. QSOs.

The GB6-PMN/X-ray CCF is dominated by Poisson noise and can be used to infer that $\sim 2\%$ of the $2 - 10$ keV background is due to 5 GHz radio sources with fluxes in excess of $50mJy$.

I would like to acknowledge useful conversations with Rob Crittenden, Ofer Lahav, Neil Turok, Insu Yi, and especially with Daniel Eisenstein. Keith Jahoda kindly supplied me with the HEAO I A2 X-ray data and several data handling programs. Much of this work was completed at Princeton University where I benefitted greatly from the subroutines of Ed Groth. This work was supported in part by NASA grant NAG 5-3015, NSF grant PHY-9222952, and the Monel Foundation.

REFERENCES

- Allen, J., Jahoda, K., & Whitlock, L. 1994, *Legacy*, 5, 27
- Almaini, O., and Fabian, A. C. 1997, *MNRAS*, in press (astro-ph/9704128)
- Almaini, O., Shanks, T., Griffiths, R. E., Boyle, B. J., Roche, N., Georgantopoulos, I., & Stewart, G. C 1997, *MNRAS*, in press (astro-ph/9704117)
- Barcons, X., Fabian, A. C., & Carrera, F. J. 1997, *MNRAS*, in press
- Becker, R. H., White, R. L., & Helfand, D. J. 1995, *ApJ*, 450, 559
- Bennett, C. L. et al. 1996, *ApJ*, 464, L1

- Boldt, E. 1987, Phys Rept, 146, 215
- Boughn, S. P., Crittenden, R. G., Turok, N. G. 1997, submitted to ApJ
- Boyle, B. J., Giffiths, R. E., Shanks, T., Stewart, G. C., & Georgantopoulos, I. 1994, MNRAS, 271, 639
- Comastri, A., Setti, G., Zamorani, G., & Hasinger, G. 1995, A & A, 296, 1
- Cress, C. M., Helfand, D. J., Becker, R. H., Gregg, M. D., & White, R. L. 1996, ApJ, 473, 7
- Dunlop, J. S. & Peacock, J. A. 1990, MNRAS, 247, 19
- Gendreau, K. C., et al. 1995, PASJ, 47, L5
- Georgantopoulos, I., Stewart, G. C., Blair, A., J., Shanks, T., Griffiths, R. E., Boyle, B. J., Almaini, O., & Roche, N. 1997, MNRAS, in press
- Gregory, P. C., Scott, W. K., Douglas, K., & Condon, J. J. 1996, ApJS, 103, 427
- Griffith, M. R., Wright, A. E., Burke, B. F., Ekers, R. D. 1994, ApJS, 90, 179
- Griffith, M. R., Wright, A. E., Burke, B. F., Ekers, R. D. 1995, ApJS, 97, 347
- Fisher, K. B., Davis, M., Strauss, M. A., Yahil, A., & Huchra, J. 1994, MNRAS, 266, 50
- Hasinger, G., Burg, R., Giacconi, R., Hartner, G., Schmidt, M., Trumper, J., & Zamorani, G. 1993, A & A, 275, 1
- Jahoda, K. 1993, Adv Space Res, 13, No 12, 231
- Jahoda, K., & Mushotzky, R. 1989, ApJ, 346, 638
- Lahav, O., Piran, T., & Treyer, M. A. 1997, MNRAS, 284, 499
- Ling, E. N., Frenk, C. S., & Barrow, J. D. 1986, MNRAS, 223, 21
- Loan, A. J., Wall, J. V., & Lahav, O. 1997, MNRAS, 286, 994
- Marshall, F. E., Boldt, E. A., Holt, S. S., Miller, R. B., Mushotzky, R. F., Rose, L. A., Rothschild, R. E., & Serlemitsos, P. J. 1980, ApJ, 235, 4
- Miyaji, T., Lahav, O., Jahoda, K., & Boldt, E. 1994, ApJ, 434, 424
- Padmanabhan, T. 1993, Structure Formation in the Universe, (Cambridge University Press, Cambridge)
- Peebles, P. J. E. 1980, The Large-Scale Structure of the Universe, (Princeton Univ Press, Princeton, NJ)

- Peebles, P. J. E. 1993, *Principles of Physical Cosmology*, (Princeton Univ Press, Princeton, NJ)
- Piccinotti, G., Mushotzky, R., Boldt, E., Marshall, F., Serlemitsos, P., & Shafer, R. 1982, *ApJ*, 253, 485
- Refregier, A., Helfand, D. J., & McMahon, R. G. 1997, *ApJ*, 477,58
- Roche, N., Shanks, T., Georgantopoulos, I., Stewart, G. C., Boyle, B. J., & Griffiths, R. E. 1995, *MNRAS*, 273, L15
- Shafer, R. A. 1983, PhD Thesis, Univ of Maryland
- Treyer, M. A., & Lahav, O. 1996, *MNRAS*, 280, 469
- White, R. L., Becker, R. H., Helfand, D. J., & Gregg, M. D. 1997, *ApJ*, 475, 479
- White, R. A. & Stemwedel, S. W. 1992, in *Astronomical Data Analysis Software and Systems I*, eds. D. M. Worrall, C. Biemesderfer, & J. Barnes (San Francisco: ASP), 379
- Wright, A. E., Griffith, M. R., Burke, B. F., & Ekers, R. D. 1994, *ApJS*, 91, 111
- Wright, A. E., Griffith, M. R., Hunt, A. J., Troup, E., Burke, B. F., & Ekers, R. D. 1994, *ApJS*, 103, 145

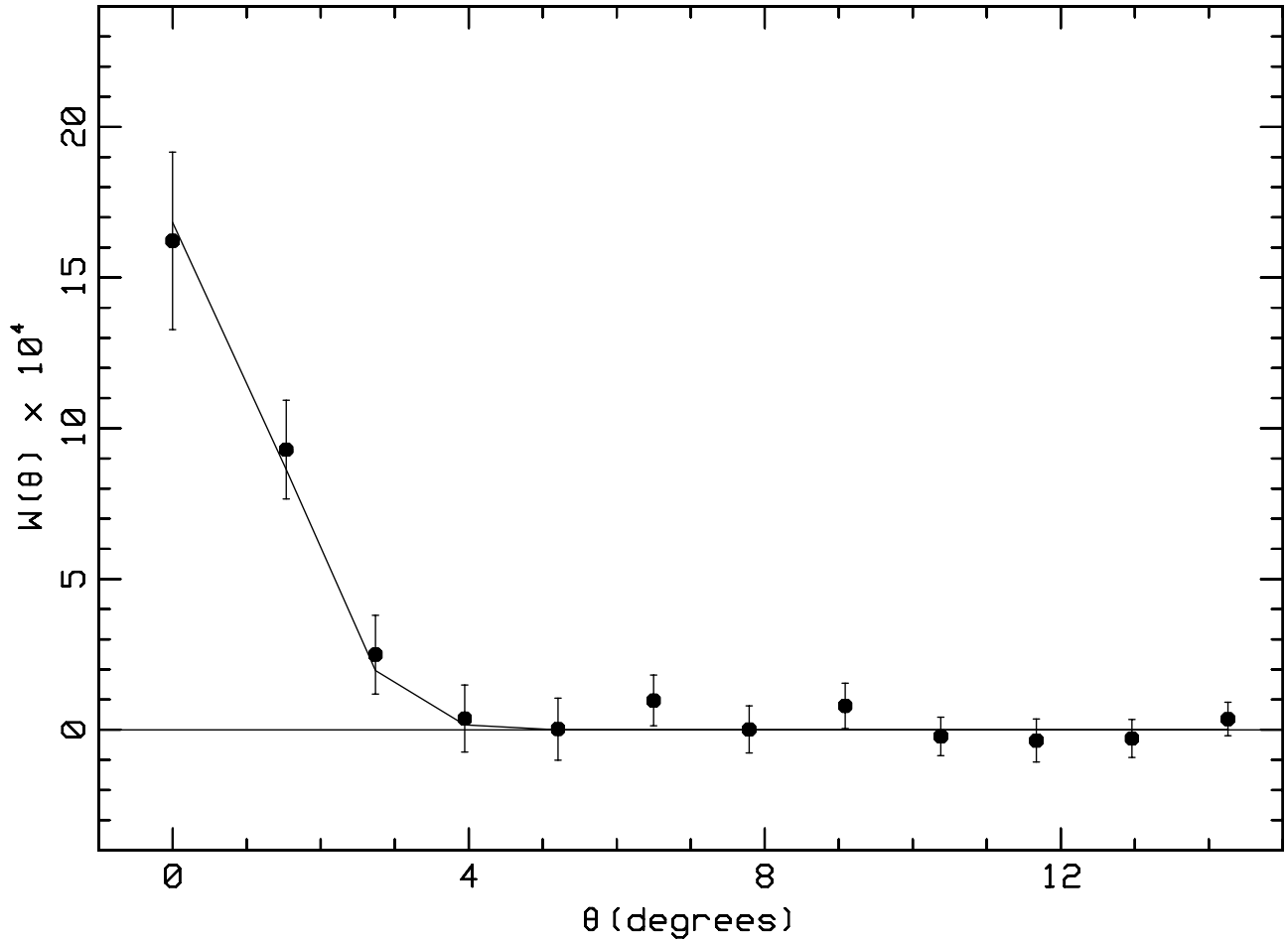


Fig. 1.— Cross-correlation function of diffuse 2 – 10 *keV* X-rays with the 5*GHz* GB6-PMN radio surveys. The errors are statistical only and are highly correlated. The curve is a fit to the profile expected for Poisson fluctuations convolved with the X-ray beam. See §4 .

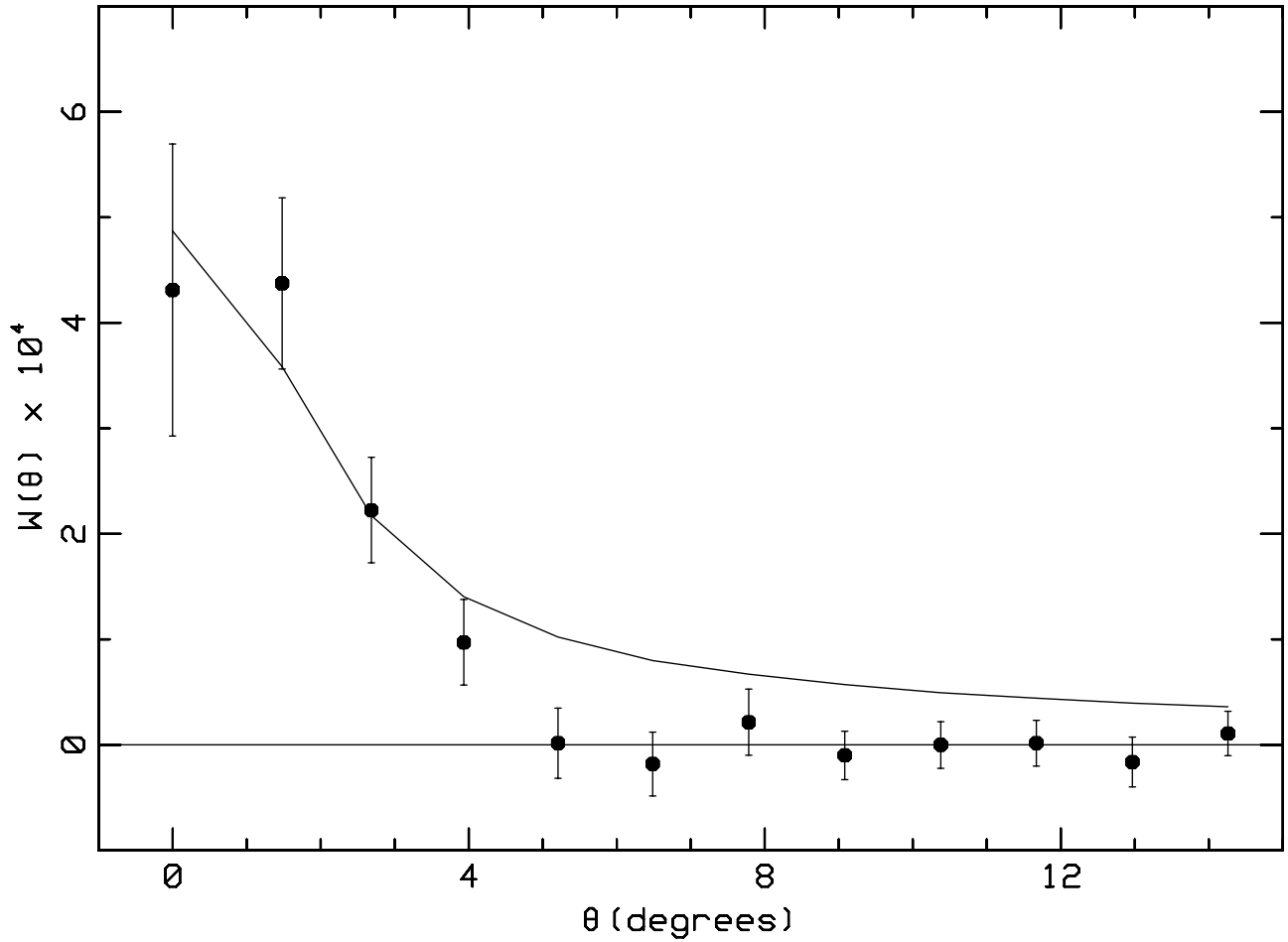


Fig. 2.— Cross-correlation function of diffuse 2 – 10 keV X-rays with the 1.4GHz FIRST radio survey. The errors are statistical only and are highly correlated. The curve is a fit to the profile expected for $\gamma = 2$ spatial clustering. See §4 .

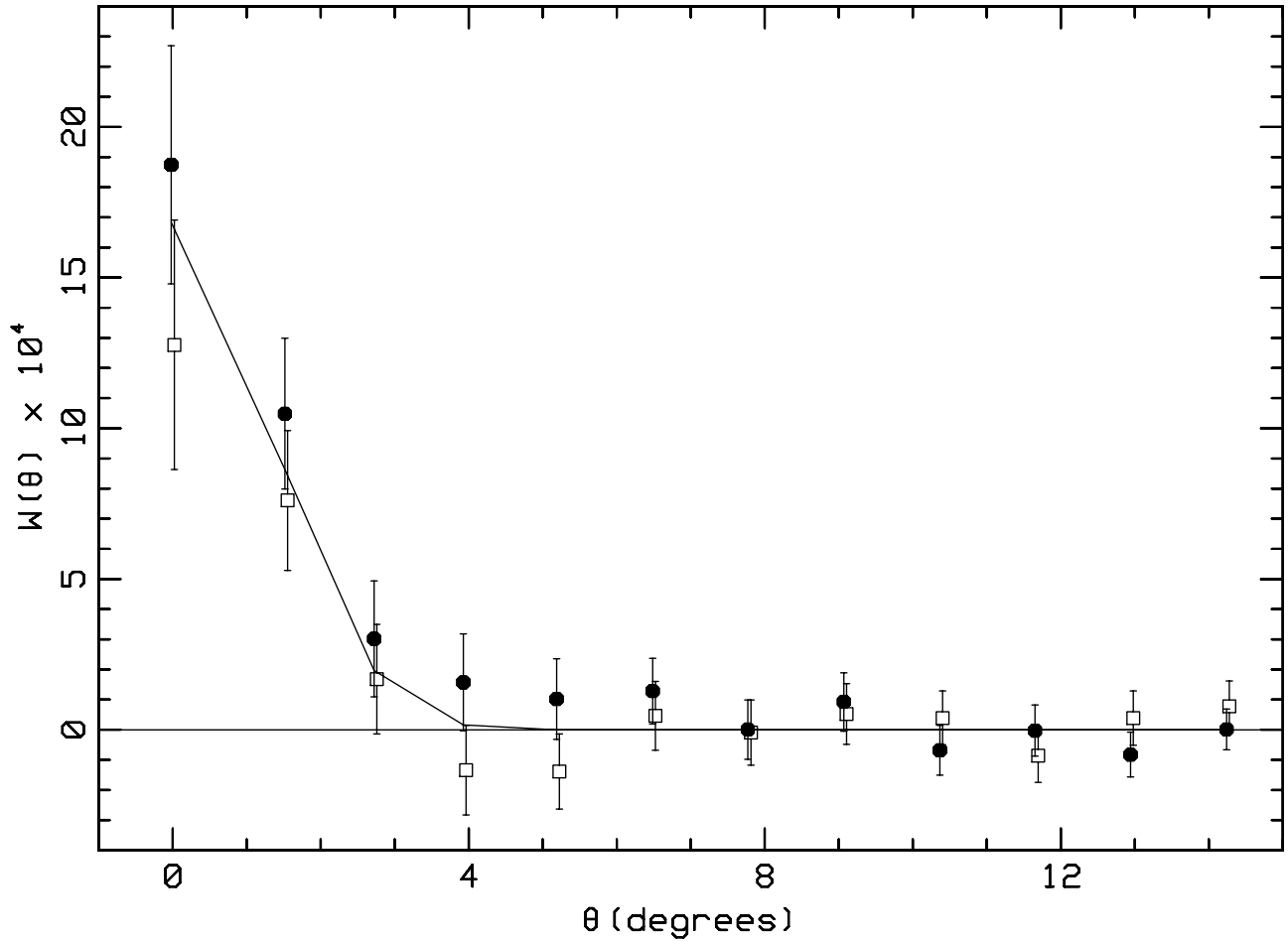


Fig. 3.— Cross-correlation function of diffuse 2 – 10 *keV* X-rays with the 5*GHz* GB6 radio survey (filled circles) and PMN survey (open squares). The errors are statistical only and are highly correlated. The curve is the same fit as in Figure 1.

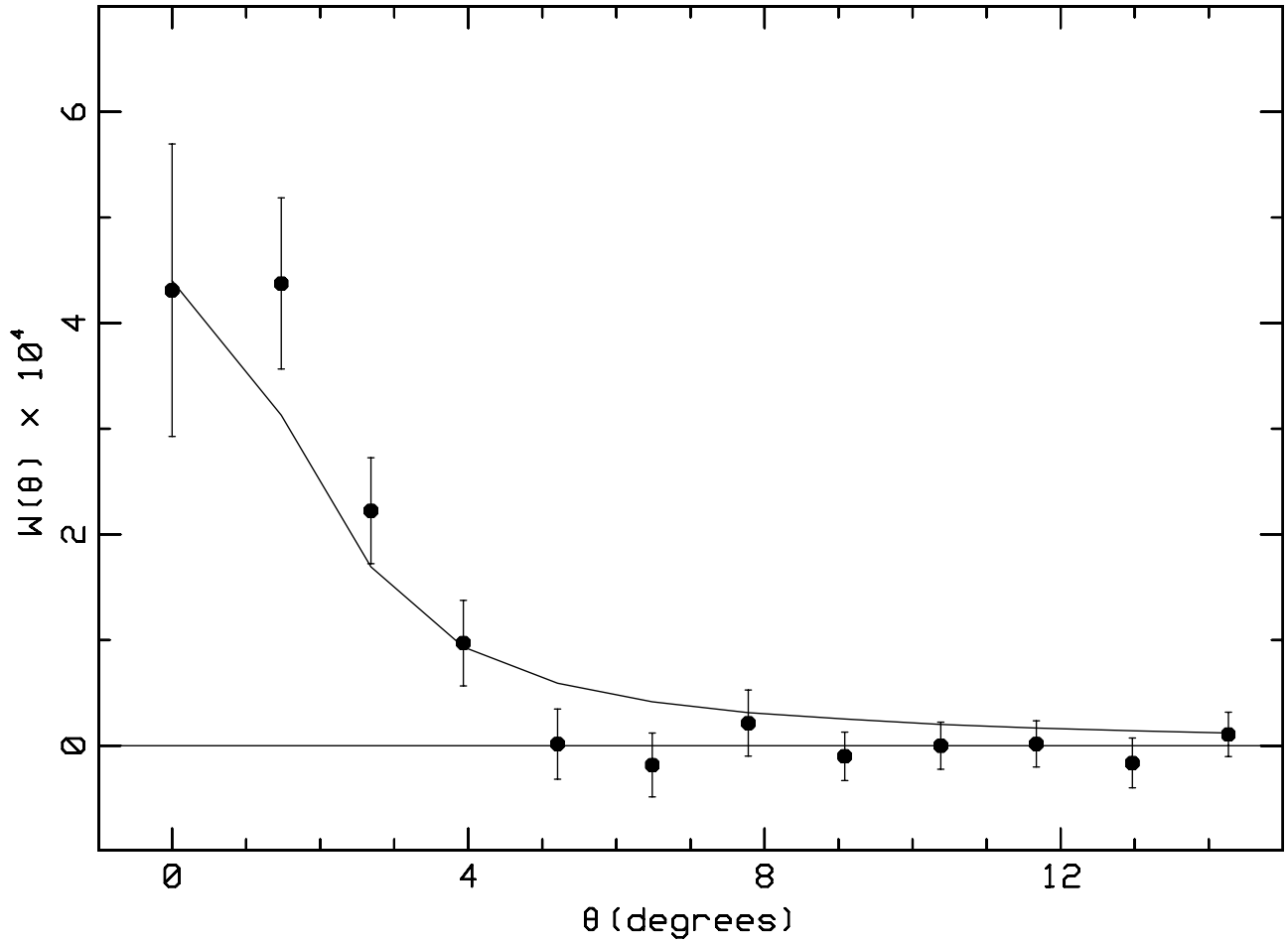


Fig. 4.— Cross-correlation function of diffuse 2 – 10 keV X-rays with the 1.4GHz FIRST radio survey. The data is the same as in Figure 2. The curve is the fit to the profile expected for $\gamma = 2$ spatial clustering cut off at a physical distance of $30h^{-1}Mpc$. See §4.

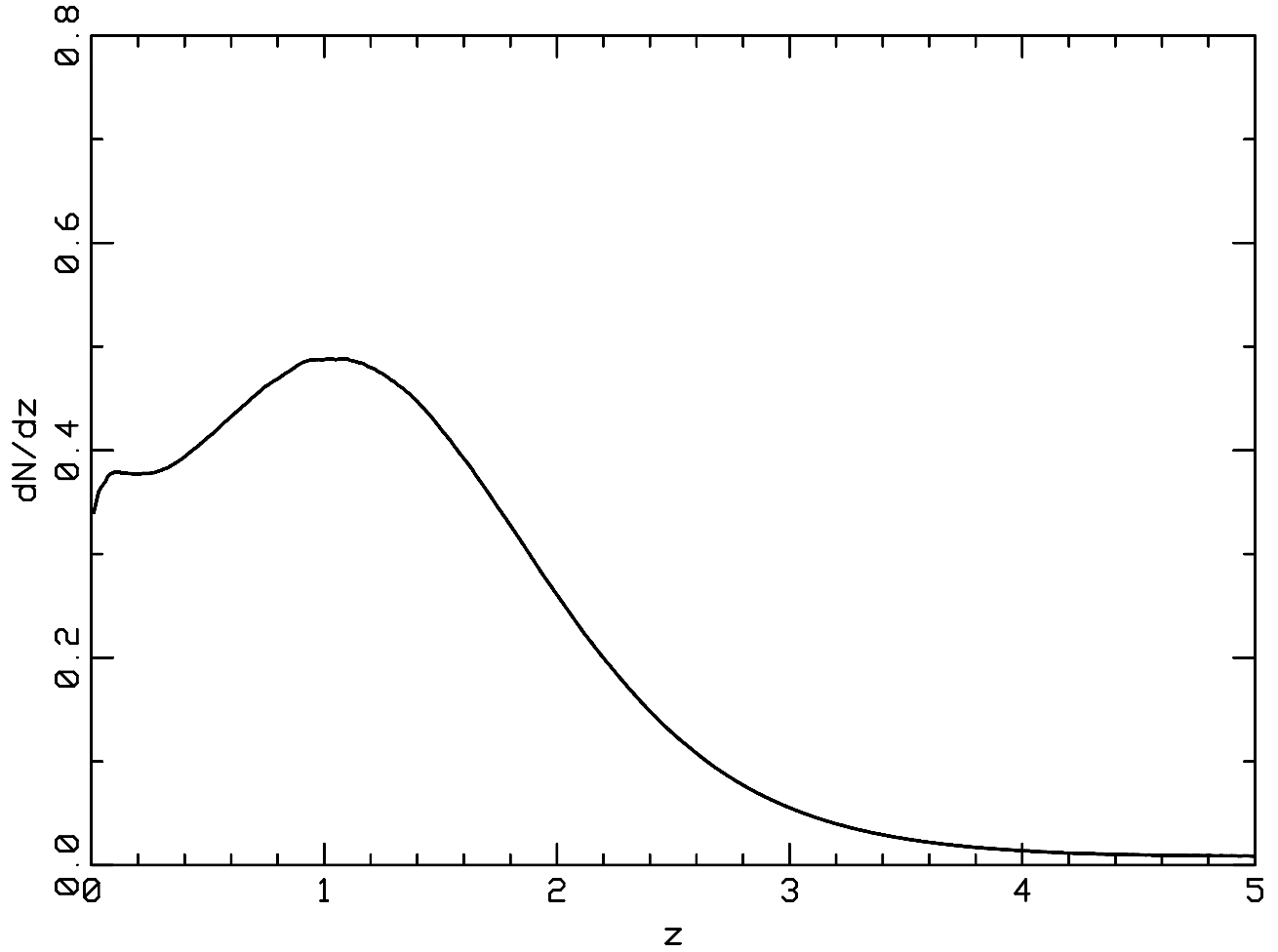


Fig. 5.— The redshift distribution of $50mJy$ flux limited $5GHz$ radio number counts predicted by the luminosity function model (model 1 MEAN-z) of Dunlop & Peacock (1994).

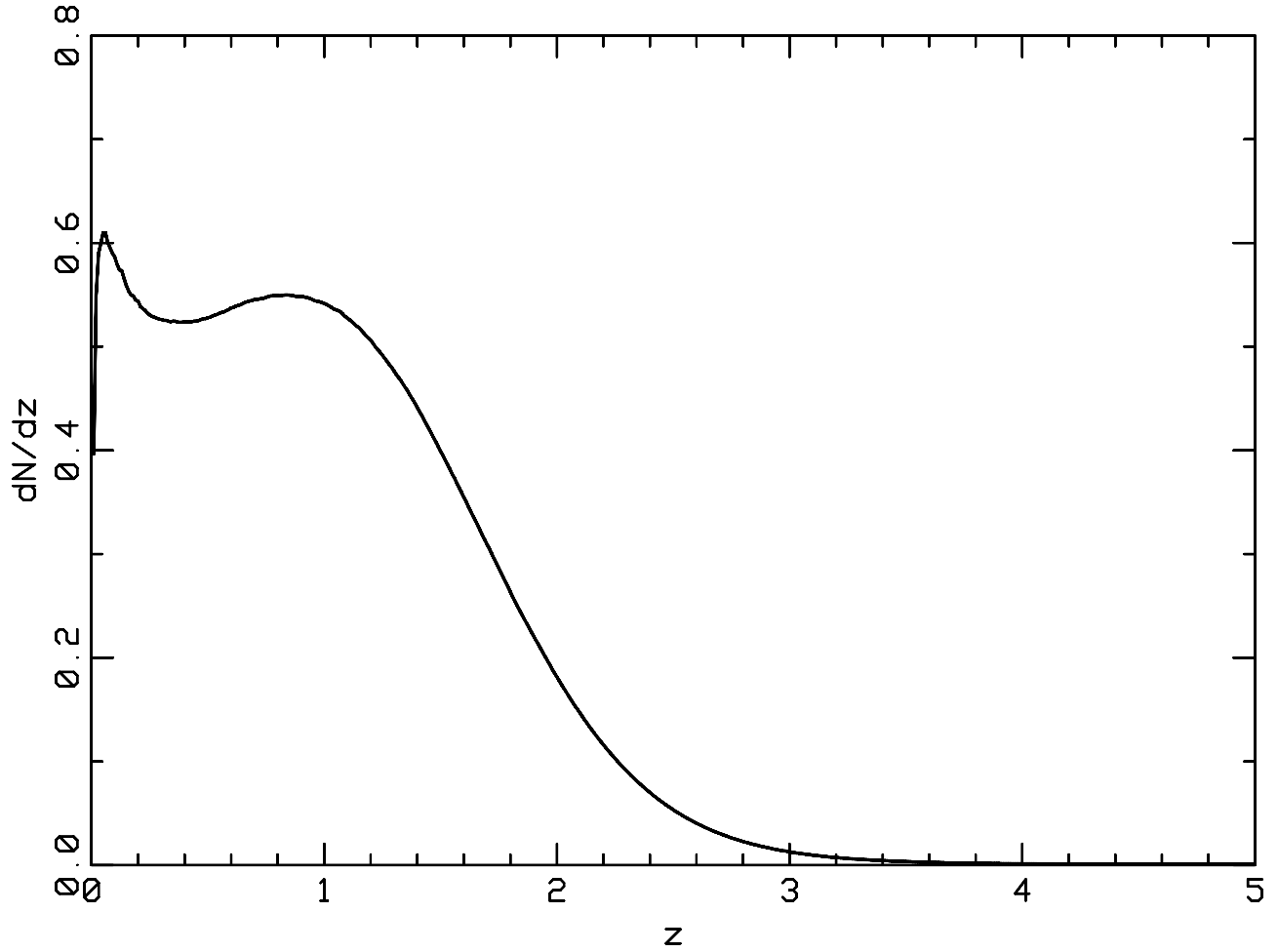


Fig. 6.— The redshift distribution of $1.5mJy$ flux limited $1.4GHz$ radio number counts predicted by the luminosity function model (model 1 MEAN- z) of Dunlop & Peacock (1994).

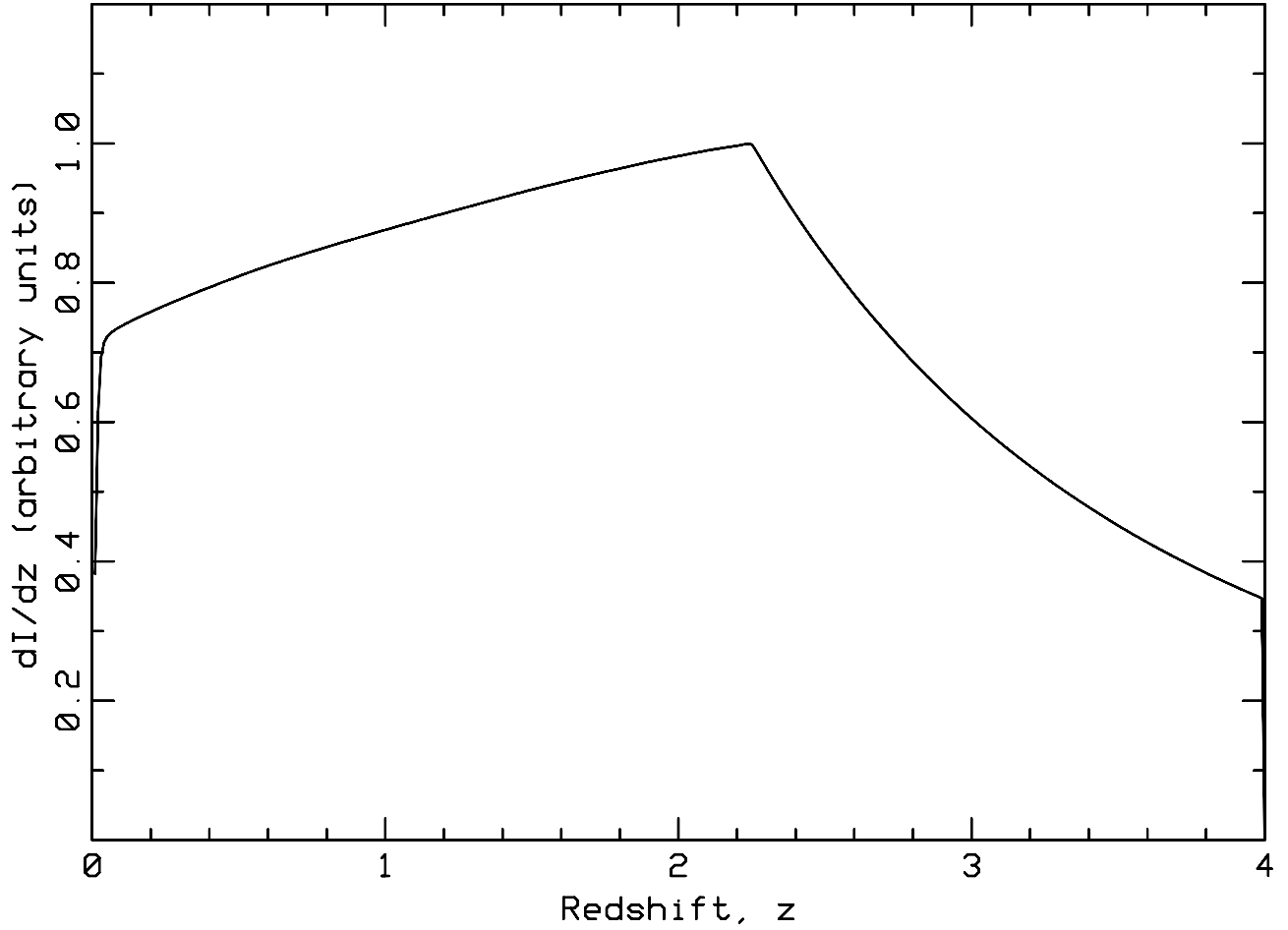


Fig. 7.— Redshift distribution of the 2–10 keV X-ray Background, dI/dz , from the unified AGN model of Comastri et al. (1995). Sources with fluxes exceeding $3 \times 10^{-11} \text{ erg s}^{-1} \text{ cm}^{-2}$ have been cut.

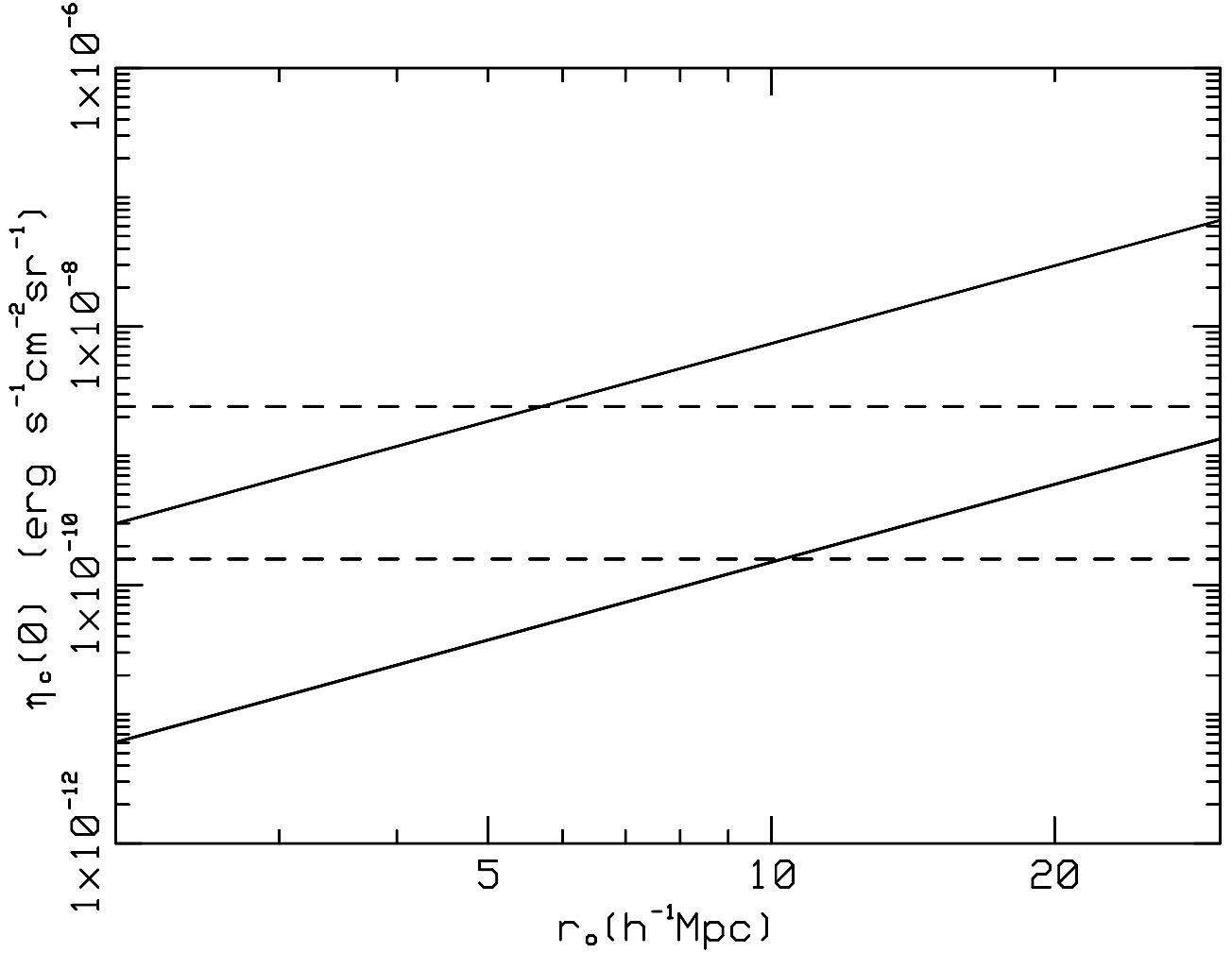


Fig. 8.— Predicted cross-correlation amplitude, $\eta_c(0)$, as a function of correlation scale length, r_0 , using the “best guess” model discussed in the text. The upper solid curve is that predicted for the FIRST/X-ray CCF and the lower solid curve for the GB6-PMN/Xray CCF. The upper dashed line corresponds to the amplitude fitted to the FIRST/X-ray data and the lower dashed line to the amplitude fitted to the GB6-PMN/X-ray data. Note: the dashed lines should be considered upper limits since Poisson fluctuations have not been corrected for. See §4 and §5.